Spin pumping by higher-order dipole-exchange spin-wave modes

Peng Wang(王鹏)[1,2,†]

[1] *College of Mathematics and Physics, Qingdao University of Science and Technology, Qingdao* 266061, *China*
[2] *Advanced Optoelectronic Materials and Technologies Engineering Laboratory of Shandong Province, Qingdao* 266061, *China*

(Received 7 June 2022; revised manuscript received 28 July 2022; accepted manuscript online 12 August 2022)

Spin pumping (SP) and inverse spin Hall effect (ISHE) driven by parametrically-excited dipole-exchange spin waves in a yttrium iron garnet film have been systematically investigated. The measured voltage spectrum exhibits a feature of the field-induced transition from parallel pumping to perpendicular pumping because of the inhomogeneous excitation geometry. Thanks to the high precision of the SP-ISHE detection, two sets of fine structures in the voltage spectrum are observed, which can correspond well to two kinds of critical points in the multimode spin-wave spectrum for magnetic films. One is the $q = 0$ point of each higher-order dispersion branch, and the other is the local minimum due to the interplay between the dipolar and exchange interactions. These fine structures on the voltage spectrum confirm the spin pumping by higher-order dipole-exchange spin-wave modes, and are helpful for probing the multimode spin-wave spectrum.

Keywords: spin pumping, parametric excitation, spin-wave spectrum, fine structures

PACS: 76.50.+g, 75.40.Gb, 75.30.Ds **DOI:** 10.1088/1674-1056/ac8922

1. Introduction

Spin waves (or magnons), which are the collective excitation of a magnetically ordered system, have drawn increasing attention due to their anticipated potential for transferring and processing information.[1–3] In the last few years, several spin-wave logic device concepts have been proposed and experimentally verified, such as spin-wave majority gates,[4] magnon transistors,[5] and spin-wave directional coupler.[6,7] Simultaneously, fascinating new phenomena such as magnon Bose–Einstein condensation,[8] magnonic supercurrents,[9] and hybrid magnetoelastic bosons[10] have been discovered, enriching the research areas of fundamental spin physics.

Recent advances in spintronics provide a new approach for the detection of spin waves: the combination of spin pumping (SP) and inverse spin Hall effect (ISHE).[11–14] Specifically, the precessing magnetization of spin waves can emit angular momentum into an adjacent normal-metal (NM) in the form of a pure-spin-current, which can then be converted to an electrically detectable charge current via the ISHE. The SP-ISHE detection method is considered to have no limitation from the spin-wave wavelength,[15,16] and therefore has the advantage of detecting spin waves in the dipole-exchange region, where the strength of the dipole–dipole interaction and the exchange interaction are comparable. Many experimental studies on this subject have been reported, such as SP driven by parametrically excited exchange magnons,[17–19] bistable exchange spin waves,[20] and magnon polarons.[21] Most of these studies have been performed using magnetic thin films, whose spin-wave spectrum has a multimode nature due to the confinement along the film normal. However, previous studies of SP driven by dipole-exchange spin waves mainly focused on the lowest spin-wave mode, which has a uniform profile along the film normal. So far, SP driven by higher-order dipole-exchange spin-wave modes with oscillating profiles along the film normal have rarely been reported.

In order to detect the higher-order dipole-exchange spin-wave modes, it is necessary to identify them on the measured SP-ISHE voltage spectrum. Some critical points in the spin-wave dispersion relation, such as local minima, maxima, and saddle points, can help with this. These points, also known as the van Hove singularities[22] (VHSs) in the density of states (DOS), can produce observable features in spectral measurements.[23] For example, in twisted graphene layers, VHSs in the electronic band structure can lead to sharp peaks in the scanning tunneling spectroscopy.[24,25] In this letter, similar behaviors were observed in the SP-ISHE detection of spin waves. The $q = 0$ points and local minima in the higher-order spin-wave dispersion branches were found to produce two sets of fine structures[26] on the measured SP-ISHE voltage spectrum. These fine structures confirm the observation of SP driven by higher-order spin-wave modes. In addition, they provide anchor points for establishing the exact correspondence between the measured SP-ISHE voltage and the multimode dipole-exchange spin-wave spectrum.

2. Experimental details

The sample used in the present study was a 3.7-μm-thick (111)-single-crystal yttrium iron garnet (YIG) film grown on

†Corresponding author. E-mail: pwang7000@163.com

© 2023 Chinese Physical Society and IOP Publishing Ltd

a gallium gadolinium garnet (GGG) substrate by liquid phase epitaxy, as shown in Fig. 1(a). A 50-μm-wide Cu strip was deposited in the middle of the YIG film used as the microstrip antenna for the spin-wave excitation. A 25-μm-wide and 10-nm-thick Pt strip was deposited 100 μm away from the microstrip antenna for the SP-ISHE detection. In order to achieve high sensitivity, a lock-in technique was used. A microwave source with a power amplifier supplies to the microstrip antenna a CW microwave, which was modulated with a frequency of 51.73 kHz. The SR830 lock-in amplifier was wired to the Pt strip to detect the voltage generated by the ISHE. The external magnetic field H is applied perpendicular to the Pt strip and the microstrip antenna. The measurements were all performed at room temperature.

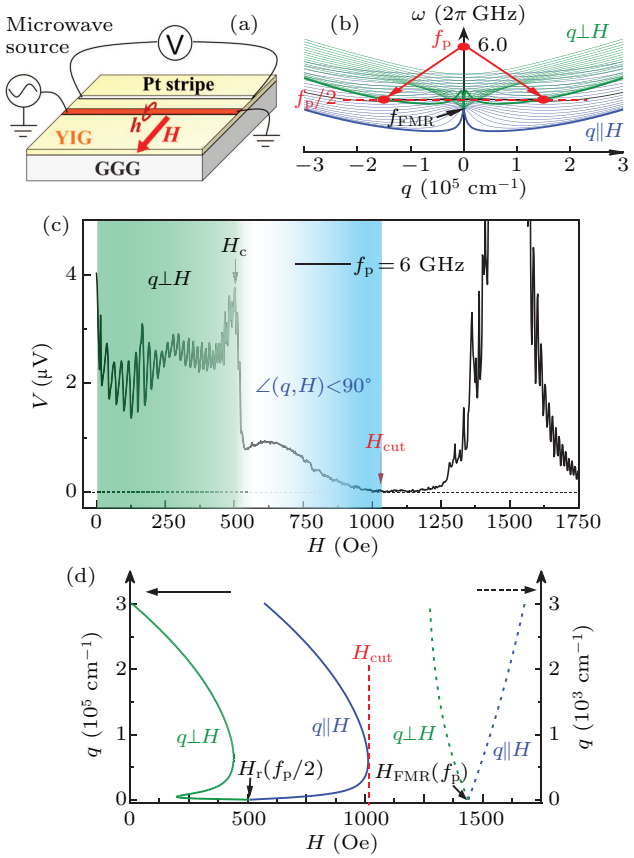


Fig. 1. (a) Schematic illustration of the experimental setup. (b) Sketch of the multi-mode spin-wave spectrum of a YIG film and the mechanism of the parametric excitation. (c) The measured ISHE voltage spectrum at the pumping frequency of 6 GHz. (d) The calculated H dependence of the in-plane wave number q of the linearly and parametrically excited spin waves for a 3.7-μm-thick YIG film under the $f_p = 6$ GHz. The unit 1 Oe = 79.5775 A·m^{-1}.

3. Results and discussion

3.1. Multimode spin-wave spectrum

The dipole-exchange spin-wave spectrum in a YIG film with a finite thickness d, which can be regarded as a series of quasi-two-dimensional systems, has a form given by Kalinikos and Slavin[27,28]

$$\omega_n^2(q) = \gamma^2 \left\{ H + \frac{2A}{M_S}\left[q^2 + \left(\frac{n\pi}{d}\right)^2\right] \right\} \times \left\{ H + \frac{2A}{M_S}\left[q^2 + \left(\frac{n\pi}{d}\right)^2\right] + 4\pi M_S F_{nn}(qd) \right\}, \quad (1)$$

where $n = 0, 1, 2, \ldots$ are the quantization numbers due to the finite film thickness, γ is the gyromagnetic ratio, A is the exchange stiffness, M_S is the saturation magnetization, q is the magnitude of in-plane wave-vector $\boldsymbol{q}$, and $F_{nn}(qd)$ is the matrix element of the magnetic dipole–dipole interaction (see supporting information S1). Figure 1(b) schematically illustrates the spin-wave spectrum of a 3.7-μm-thick YIG film and the mechanism of the parametric excitation. The spectrum should include all possible directions of the spin-wave propagation. Here, for simplicity, we only draw the directions of $\boldsymbol{q}$ parallel (blue curves) and perpendicular (green curves) to H in Fig. 1(b). The two thick curves represent the lowest $n = 0$ branches in these two directions. Under linear excitation, where the frequency of the excited spin wave is the same as the microwave pumping frequency f_p, only magnons distributed in a small wave vector range near the $\boldsymbol{q} = 0$ uniform-mode can be excited.[29] In contrast, the parametric excitation technique can excite magnon pairs with half the microwave frequency $f_p/2$ and opposite wave vectors $\pm\boldsymbol{q}$ in a large wave vector range of the spectrum. Both linearly and parametrically excited magnons with small or large wave vectors can drive spin pumping and then be detected as a dc voltage by the ISHE of the Pt strip.[19,30]

During the measurement, the Cu microstrip can excite different steady spin-wave modes under different applied magnetic fields. These modes are usually distributed over the entire YIG film,[31] and are sufficient to cover the Pt strip. These different modes have different excitation efficiencies, so the magnetic moments beneath the Pt strip have different precession amplitudes, resulting in different voltages. Therefore, the measured voltage spectrum can reflect the information of the spin-wave spectrum.

3.2. The measured ISHE voltage spectrum

Figure 1(c) shows the dependence of the measured ISHE voltage V on H with $f_p = 6$ GHz and an input microwave power about 300 mW. A background voltage V_b, which is associated with the spin Seebeck effect[32] and almost independent of the value of H in our measurement range,[33,34] is subtracted from the measured voltage V_m: $V = V_m - V_b$. The entire spin-wave spectrum and the ferromagnetic resonance (FMR) frequency f_{FMR} in Fig. 1(b) can be shifted up or down along y axis by tuning the magnitude of H. As H is scanned from high field to approach ~ 1500 Oe (1 Oe = 79.5775 A·m^{-1}) to fulfill $f_p \approx f_{FMR}$, the linear excitation of the uniform FMR mode occurs, resulting in the relatively large SP-ISHE voltage in Fig. 1(c). In addition to the peak arising from the FMR, multiple peaks are observed between 1250 Oe and 1750 Oe. These signals are attributed to the SP-ISHE voltage driven by the standing spin waves due to the confinement of the sample

plane and thickness direction of the rectangular sample.[35,36] When the dispersion curves move further down with decreasing H to intersect the line $f_p/2$, the parametric excitation begins, as evidenced by the emergence of the ISHE voltage in Fig. 1(c) below the cutoff field $H_{cut} = 1030$ Oe. H_{cut} corresponds to the applied field at which the lowest point of the entire spin-wave spectrum intersects the line $f_p/2$. When H is greater than H_{cut}, the dispersion curves are above $f_p/2$. Only if H is less than H_{cut}, the dispersion curves can intersect with $f_p/2$. Therefore, the parametric excitation can only occur below H_{cut}.

Figure 1(d) shows the calculated dependence of the in-plane wave-vector q on H from Eq. (1) for the linear excitation (with fixed $\omega = 2\pi \cdot f_p$) and parametric excitation (with fixed $\omega = 2\pi \cdot f_p/2$). Only the lowest $n = 0$ mode and the directions of $\boldsymbol{q}||\boldsymbol{H}$ and $\boldsymbol{q}\perp\boldsymbol{H}$ are shown. $H_{FMR}(f_p)$ and $H_r(f_p/2)$ on the abscissa are the calculated resonance fields for the linear and parametric excitation, respectively. As can be seen from the comparison between Figs. 1(c) and 1(d), the voltage signals from the linearly-excited spin waves appear in a small range of q, with a maximum value of about 3×10^3 cm^{-1}, which is in the magnetostatic wave range. In contrast, the voltage signals from the parametrically-excited spin waves cover much large range of q, with a maximum value of about 3×10^5 cm^{-1}, which is two orders larger than that of the linear excitation and is in the dipole-exchange region. In the following, we focus on analyzing the parametrically-excited SP-ISHE voltage spectrum in the $H < H_{cut}$ part.

3.3. Transition from parallel to perpendicular parametric pumping

The field dependence of V for $H < H_{cut}$ as shown in Fig. 1(c) exhibits the typical feature of the field-induced transition from parallel parametric pumping (the pump microwave field $\boldsymbol{h}||\boldsymbol{H}$)[37,38] to perpendicular parametric pumping ($\boldsymbol{h}\perp\boldsymbol{H}$)[39,40] with decreasing H. As well studied in Ref. [41], the transition is attributed to the excitation geometry of the microstrip antenna. Our SP-ISHE measurement results in Fig. 1(c) are in good agreement with the threshold pump power measurement results in Ref. [41]. At the critical field H_c, which is close to $H_r(f_p/2)$, the spin waves with $q \approx 0$ are excited. Because the threshold power of parametric excitation at H_c is the lowest, the corresponding ISHE voltage V shows a maximum value. Below H_c, the parallel pumping dominates, and spin waves with $\boldsymbol{q}\perp\boldsymbol{H}$ are mainly excited. These spin waves propagate along the microstrip antenna, *i.e.*, they are localized around the pump region, leading to the relatively-high excitation efficiency and hence a relatively large V [the green area of Fig. 1(c)]. Above H_c, the perpendicular pumping gradually dominates, and $\boldsymbol{q}$ of the mainly-excited spin waves has an angle $\angle(\boldsymbol{q}, \boldsymbol{H})$ smaller than 90° [the blue area of Fig. 1(c)]. The sharp voltage drop above H_c is due to the energy leakage from the pumping region by spin-wave components propagating perpendicular to the microstrip antenna. As the applied field approaching to H_{cut}, the threshold power of the parametric pumping gradually going to infinity, with the ISHE voltage V tends to zero at H_{cut}.

3.4. Fine structures on the ISHE voltage spectrum

The above discussion only considers the lowest $n = 0$ spin-wave mode to describe the overall shape of the voltage spectrum. However, in addition to that, a remarkable feature is that a series of distinct peaks are observed below H_c. To understand the origin of these peaks, we further performed the spin pumping measurements with $f_p = 4$ GHz, 5 GHz, and 7 GHz. The results are shown in Fig. 2, where, for comparison, we redefined the abscissa relative to $H_r(f_p/2)$, *i.e.*, $\Delta H = H - H_r(f_p/2)$. One can see that these peaks below $H_r(f_p/2)$ are located at the same ΔH for different f_p and disappear until H is too small to saturate the magnetization. The dotted vertical lines mark the locations of these peaks, showing that the spacing between the neighboring peaks gets larger with decreasing ΔH. Above $H_r(f_p/2)$, new peaks emerge with decreasing f_p down to 4 GHz and 5 GHz, identified by the arrows in Fig. 2. In contrast to the peaks below f_p, these peaks have a roughly equally spacing and the spacing decreases with decreasing f_p. Obviously, these two kinds of fine structures on the voltage spectrum cannot be explained by considering only the lowest $n = 0$ spin-wave mode, indicating that the higher-order diploe-exchange spin-wave modes also contribute to the spin pumping and form these observable voltage peaks.

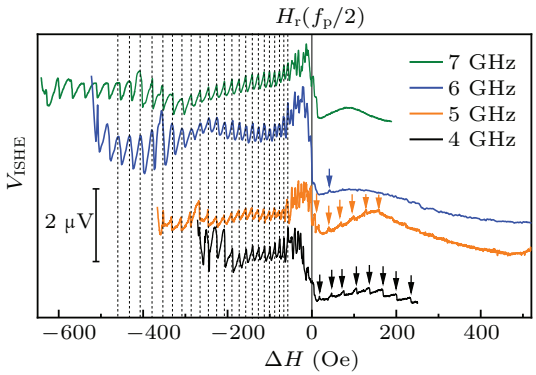


Fig. 2. The measured parametrically excited ISHE voltage spectra at the pumping frequency f_p from 4 GHz to 7 GHz. The abscissa $\Delta H = H - H_r(f_p/2)$, where $H_r(f_p/2)$ is the ferromagnetic resonance field for each $f_p/2$.

3.5. Left V_{ISHE} peaks

Owing to the confinement of the finite YIG thickness, the parametrically-excited spin waves can form standing spin waves in the thickness direction. The standing spin waves correspond to the in-plane wave-vector $q = 0$ in Eq. (1), leading to $F_{nn}(0) = 1$ and thus have an expression $\omega^2(0) = \gamma^2[H_n + 2A/M_S(n\pi/d)^2][H_n + 2A/M_S(n\pi/d)^2 + 4\pi M_S]$, where H_n is

the n-th field of the occurrence of the spin wave resonance (SWR). For a fixed frequency ω, the relative SWR field, $\Delta H_n = H_n - H_r(f_p/2)$, fulfills the equation

$$\Delta H_n = -\frac{2A}{M_S}\left(\frac{n\pi}{d}\right)^2. \tag{2}$$

These derived ΔH_n ($n = 1, 2, 3, \ldots$) correspond exactly to the voltage peaks on the left of Fig. 2.

Figure 3(a) shows the enlarged view of the left peaks from $n = 20$ to 23 for $f_p = 7$ GHz data, where the red dashes mark the peak positions. The dependence of the n-th peak's field position ΔH_n (left) on number n (form 12 to 34), extracted from the 7-GHz data in Fig. 2, is shown by the black dots in Fig. 3(b). As for the first 11 peaks, because they are close to $H_r(f_p/2)$ and their shapes are not regular, their positions cannot be well identified. The red curve in Fig. 3(b) shows the fitting result with Eq. (2). The fitting yields $A \approx 3.82$ pJ/m, consistent with the previous reports.[42] The well fit confirms that the left fine structures originate from the SWR of the parametric excited spin wave.

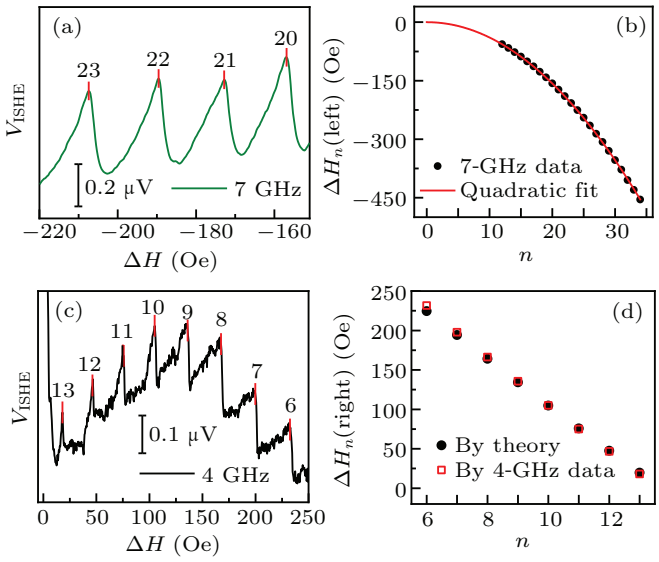


Fig. 3. (a) Magnified view of the peaks in the $\Delta H < 0$ region at $f_p = 7$ GHz. (b) Dependence of the peak position ΔH_n (left) on index n from the 7-GHz data. The red line shows the quadratic fitting. (c) Magnified view of the peaks in the $\Delta H > 0$ region at $f_p = 4$ GHz. (d) Dependence of the peak position ΔH_n (right) on index n from the 4-GHz data. The black dots show the calculated values from Eq. (1).

3.6. Right V_{ISHE} peaks

As for the fine structures in the perpendicular pumping ($\Delta H > 0$) region marked by arrows in Fig. 2, we attributed them to the spin pumping by the parametric-excited spin waves with wave vectors at the local minima of the higher-order dispersion curves, which correspond to the minima of the $\boldsymbol{q}||\boldsymbol{H}$ blue curves shown in Fig. 1(b). At these points, the group velocity of spin waves v_g is zero, and they originate from the interplay between the dipolar and exchange interactions. The enlarged view of these fine structures for the $f_p = 4$ GHz data is shown in Fig. 3(c), in which the red dashes mark their peak positions. The peaks show a sharp step-like shape and are almost equidistant spacing. The dependence of the peak position ΔH_n (right) on number n (form 6 to 13) extracted from Fig. 3(c) are plotted in Fig. 3(d). To prove that the right peaks come from the local minima of the dispersion curves, we carried out numerical calculations on Eq. (1) by finding the magnetic field values with $dH_n/dq = 0$, *i.e.*, $v_g = 0$, at fixed ω. The calculated ΔH_n values at $\omega = 2\pi \times 4$ GHz from $n = 6$ to 13 are shown by the black dots in Fig. 3(d). One can see that the measured values match well with the calculated ones, strongly suggesting that the peaks in the $\Delta H > 0$ region are indeed from the local minima of the higher-order dispersion branches.

3.7. ISHE voltage spectrum vs spin-wave spectrum

The local minimum in the dispersion relationship is a kind of VHS in the DOS. In our case, each higher-order dispersion branch with index n can be regarded as a quasi-two-dimensional system. In a two-dimensional system, the DOS at a minimum has a step function singularity.[23] The measured SP voltage V_{ISHE} depends on the number of the excited magnons,[19] which is proportional to the magnon DOS. This may be the reason for the step-like feature of the right V_{ISHE} peaks corresponding to the local minima in Fig. 3(c).

In fact, the $q = 0$ point in each higher-order dispersion branch can also be regarded as VHS. When the order index n is small except zero, the $q = 0$ point is usually a saddle point (see supporting information S2). In a quasi-two-dimensional system, the DOS at a saddle point is logarithmically divergent, and can lead to peaks in spectral measurements.[43] Therefore, from another perspective, the left V_{ISHE} peaks corresponding to the $q = 0$ points can also be considered to originate from the singularity of DOS at VHS.

From the above discussion, we can conclude that the two sets of fine structures observed in the ISHE voltage spectrum correspond to two kinds of critical points in the multimode spin-wave spectrum. One is the point where the in-plane wave vector $q = 0$, *i.e.*, the starting point of each higher-order dispersion branch, which is mainly determined by the exchange interaction. The other is the point where q satisfies $v_g = 0$, *i.e.*, the local minimum point of each higher-order dispersion branch, which is jointly determined by the dipole and exchange interactions. These fine structures provide anchor points for establishing the exact correspondence between the measured SP-ISHE voltage and the multimode dipole-exchange spin-wave spectrum.

Figure 4(a) shows the calculated H dependence of q from the dipole-exchange spin-wave theory Eq. (1) with fixed $\omega = 2\pi \times 2.5$ GHz. The first 31 dispersion branches from $n = 0$ to 30 are calculated, and only the directions of $\boldsymbol{q}||\boldsymbol{H}$ (blue

curves) are drawn for simplicity. Figure 4(b) shows the corresponding parametrically-excited voltage results measured at $f_p = 5$ GHz. It can be intuitively seen that the voltage spectrum agrees very well with the dispersion curves calculated by the dipole-exchange spin-wave theory. H_{cut} in Fig. 4(b) corresponds well to the $dH/dq = 0$ point of the lowest $n = 0$ dispersion branch. The fine structures above $H_r(f_p/2)$ correspond well to the $dH/dq = 0$ points of the $n = 7$ to 15 higher-order dispersion branches. The fine structures below $H_r(f_p/2)$ exactly match with the $q = 0$ points of each dispersion branch. These results confirm that the SP-ISHE is a powerful method to probe the multimode spin-wave spectrum.

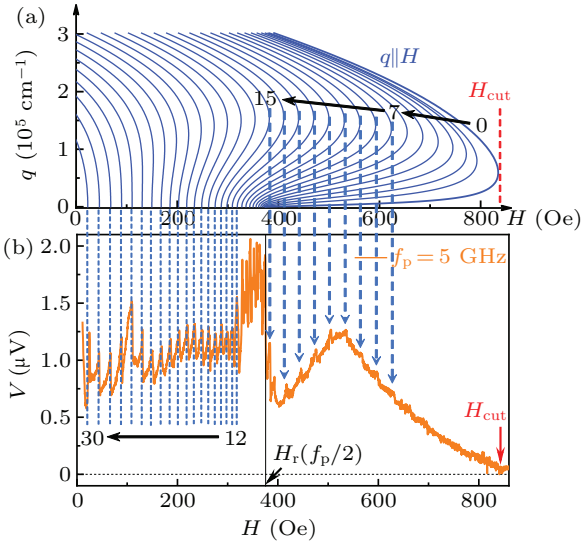


Fig. 4. (a) The calculated H dependence of the in-plane wave number q of the multimode spin waves for a 3.7-μm-thick YIG film with fixed $\omega = 2\pi \times 2.5$ GHz. (b) The measured parametrically excited ISHE voltage spectrum at $f_p = 5$ GHz. The dotted lines mark the correspondence between them.

4. Conclusion

In conclusion, we have systematically studied the spin pumping and ISHE driven by parametrically-excited spin waves in a YIG film. The shape of the measured voltage spectrum indicates the transition from parallel pumping to perpendicular pumping due to the excitation geometry. Two sets of fine structures on the voltage spectrum are observed, and are proved to correspond to two kinds of critical points in the multimode spin-wave spectrum. These fine structures confirm the spin pumping by the higher-order dipole-exchange spin-wave modes. In addition, our results provide a simple electrical detection method for probing the dispersion relation of the parametrically-excited multimode dipole-exchange spin waves.

Acknowledgement

Project supported by the National Natural Science Foundation of China (Grant No. 11904194).

References

[1] Chumak A V, Vasyuchka V I, Serga A A and Hillebrands B 2015 *Nat. Phys.* **11** 453
[2] Cornelissen L J, Liu J, Duine R A, Youssef J Ben and van Wees B J 2015 *Nat. Phys.* **11** 1022
[3] Madami M, Bonetti S, Consolo G, Tacchi S, Carlotti G, Gubbiotti G, Mancoff F B, Yar M A and Åkerman J 2011 *Nat. Nanotechnol.* **6** 635
[4] Fischer T, Kewenig M, Bozhko D A, Serga A A, Syvorotka I I, Ciubotaru F, Adelmann C, Hillebrands B and Chumak A V 2017 *Appl. Phys. Lett.* **110** 152401
[5] Chumak A V, Serga A A and Hillebrands B 2014 *Nat. Commun.* **5** 4700
[6] Wang Q, Pirro P, Verba R, Slavin A, Hillebrands B and Chumak A V 2018 *Sci. Adv.* **4** e1701517
[7] Wang Q, Kewenig M, Schneider M, Verba R, Kohl F, Heinz B, Geilen M, Mohseni M, Lägel B, Ciubotaru F, Adelmann C, Dubs C, Cotofana S D, Dobrovolskiy O V, Brächer T, Pirro P and Chumak A V 2020 *Nat. Electron.* **3** 765
[8] Demokritov S O, Demidov V E, Dzyapko O, Melkov G A, Serga A A, Hillebrands B and Slavin A N 2006 *Nature* **443** 430
[9] Bozhko D A, Serga A A, Clausen P, Vasyuchka V I, Heussner F, Melkov G A, Pomyalov A, L'vov V S and Hillebrands B 2016 *Nat. Phys.* **12** 1057
[10] Bozhko D A, Clausen P, Melkov G A, L'vov V S, Pomyalov A, Vasyuchka V I, Chumak A V, Hillebrands B and Serga A A 2017 *Phys. Rev. Lett.* **118** 237201
[11] Tserkovnyak Y, Brataas A and Bauer G E W 2002 *Phys. Rev. B* **66** 224403
[12] Kajiwara Y, Harii K, Takahashi S, Ohe J, Uchida K, Mizuguchi M, Umezawa H, Kawai H, Ando K, Takanashi K, Maekawa S and Saitoh E 2010 *Nature* **464** 262
[13] Saitoh E, Ueda M, Miyajima H and Tatara G 2006 *Appl. Phys. Lett.* **88** 182509
[14] Chumak A V, Serga A A, Jungfleisch M B, Neb R, Bozhko D A, Tiberkevich V S and Hillebrands B 2012 *Appl. Phys. Lett.* **100** 082405
[15] Ando K, Ieda J, Sasage K, Takahashi S, Maekawa S and Saitoh E 2009 *Appl. Phys. Lett.* **94** 262505
[16] Fukami M, Tateno Y, Sekiguchi K and Ando K 2016 *Phys. Rev. B* **93** 184429
[17] Sandweg C W, Kajiwara Y, Chumak A V, Serga A A, Vasyuchka V I, Jungfleisch M B, Saitoh E and Hillebrands B 2011 *Phys. Rev. Lett.* **106** 216601
[18] Ando K, An T and Saitoh E 2011 *Appl. Phys. Lett.* **99** 092510
[19] Kurebayashi H, Dzyapko O, Demidov V E, Fang D, Ferguson A J and Demokritov S O 2011 *Appl. Phys. Lett.* **99** 162502
[20] Ando K and Saitoh E 2012 *Phys. Rev. Lett.* **109** 026602
[21] Hayashi H and Ando K 2018 *Phys. Rev. Lett.* **121** 237202
[22] Van Hove L 1953 *Phys. Rev.* **89** 1189
[23] Bassani F, Parravicini G P, Ballinger R A and Birman J L 1976 *Phys. Today* **29** 58
[24] Li G, Luican A, Lopes dos Santos J M B, Castro Neto A H, Reina A, Kong J and Andrei E Y 2010 *Nat. Phys.* **6** 109
[25] Brihuega I, Mallet P, González-Herrero H, Trambly de Laissardière G, Ugeda M M, Magaud L, Gómez-Rodríguez J M, Ynduráin F and Veuillen J Y 2012 *Phys. Rev. Lett.* **109** 196802
[26] Zil'berman P, Golubev N and Temiryazev A 1990 *J. Exp. Theor. Phys.* **2** 353
[27] Kalinikos B A and Slavin A N 1986 *J. Phys. C: Solid State Phys.* **19** 7013
[28] Jorzick J, Krämer C, Demokritov S O, Hillebrands B, Bartenlian B, Chappert C, Decanini D, Rousseaux F, Cambril E, Sondergard E, Bailleul M, Fermon C and Slavin A N 2001 *J. Appl. Phys.* **89** 7091
[29] Kalinikos B A 1980 *IEE Proc. H Microwaves, Opt. Antennas* **127** 4
[30] Manuilov S A, Du C H, Adur R, Wang H L, Bhallamudi V P, Yang F Y and Hammel P C 2015 *Appl. Phys. Lett.* **107** 042405
[31] Demidov V E, Hansen U H and Demokritov S O 2007 *Phys. Rev. Lett.* **98** 157203
[32] Uchida K, Adachi H, Ota T, Nakayama H, Maekawa S and Saitoh E 2010 *Appl. Phys. Lett.* **97** 172505
[33] Ritzmann U, Hinzke D, Kehlberger A, Guo E J, Kläui M and Nowak U 2015 *Phys. Rev. B* **92** 174411
[34] Kikkawa T, Shen K, Flebus B, Duine R A, Uchida K, Qiu Z, Bauer G E W and Saitoh E 2016 *Phys. Rev. Lett.* **117** 207203

[35] Sandweg C W, Kajiwara Y, Ando K, Saitoh E and Hillebrands B 2010 *Appl. Phys. Lett.* **97** 252504
[36] Chen Y S, Lin J G, Huang S Y and Chien C L 2019 *Phys. Rev. B* **99** 220402
[37] Schlömann E, Green J J and Milano U 1960 *J. Appl. Phys.* **31** S386
[38] Nguyen H T and Cottam M G 2014 *Phys. Rev. B* **89** 144424
[39] Suhl H 1957 *J. Phys. Chem. Solids* **1** 209
[40] Wiese G, Kabos P and Patton C E 1995 *Phys. Rev. B* **51** 15085
[41] Neumann T, Serga A A, Vasyuchka V I and Hillebrands B 2009 *Appl. Phys. Lett.* **94** 192502
[42] Klingler S, Chumak a V, Mewes T, Khodadadi B, Mewes C, Dubs C, Surzhenko O, Hillebrands B and Conca A 2015 *J. Phys. D: Appl. Phys.* **48** 015001
[43] Yuan N F Q, Isobe H and Fu L 2019 *Nat. Commun.* **10** 5769
[44] Cottam M G 1994 *Linear and Nonlinear Spin Waves in Magnetic Films and Superlattices* (World Scientific)
[45] Lin F, Zhang S, Zhao G, Li H, Zong W and Li S 2020 *Chin. Phys. B* **29** 067601